Applied Ocean Research 38 (2012) 92–99

Contents lists available at SciVerse ScienceDirect

Applied Ocean Research

journal homepage: www.elsevier.com/locate/apor

# Experimental wave termination in a 2D wave tunnel using a cycloidal wave energy converter

S.G. Siegel*, C. Fagley, S. Nowlin

*Department of Aeronautics, 2410 Faculty Drive, US Air Force Academy, CO 80840, USA*

ARTICLE INFO

*Article history:*
Received 9 March 2012
Received in revised form 11 May 2012
Accepted 11 July 2012

*Keywords:*
Wave energy conversion
Cycloidal turbine
Deep ocean wave
Cycloidal wave energy converter
Wave flume
Experiment

ABSTRACT

A lift based cycloidal wave energy converter (CycWEC) is investigated in a 1:300 scale two-dimensional wave flume experiment. This type of wave energy converter consists of a shaft with one or more hydrofoils attached eccentrically at a radius. The main shaft is aligned parallel to the wave crests and submerged at a fixed depth. The operation of the CycWEC both as a wave generator as well as a wave-to-shaft energy converter interacting with straight crested waves is demonstrated. The geometry of the converter is shown to be suitable for wave termination of straight crested harmonic and irregular waves. The impact of design parameters such as device size, submergence depth, and number of hydrofoils on the performance of the converter is shown. For optimal parameter choices, experimental results demonstrate energy extraction efficiencies of more than 95% of the incoming wave energy. This is achieved using feedback control to synchronize the rotation of the CycWEC to the incoming wave, and adjusting the blade pitch angle in proportion to the wave height. Due to the ability of the CycWEC to generate a single sided wave with few harmonic waves, little energy is lost to waves radiating in the up-wave and down-wave directions.



## 1. Introduction

Among renewable energy, wave power is one of the most abundant sources on earth. The World Energy Council, according to Boyle [1], has estimated the world wide annual amount of wave power energy at 17.5 PWh (Peta Watt hours = $10^{12}$ kWh). This is comparable to annual worldwide electric energy consumption, which is currently estimated at 16 PWh. Thus, wave power has the potential to provide a large portion of the world's electric energy needs if it can be tapped efficiently. Other advantages of wave power include its power density, predictability, and location. Since a large portion of the world's population lives close to ocean shores, the distance between energy production and consumption is minimized, reducing transmission losses. Thus, wave power is an ideal energy source for efficiently providing renewable energy to densely populated coastal areas.

Given the attractive features of wave energy as an alternative energy source, it has received significant attention in the scientific community over time. While a comprehensive review of all relevant publications would be prohibitively long, the reader is instead referred to comprehensive reviews published by McCormick [2], Mei [3] or, most recently, Cruz [4]. The following discussion will instead focus only on select sources most pertinent to the current work.

There have been various wave termination designs reported in literature, with the most well-known devices being the Salter Duck [5] and the Bristol or Evans cylinder [6]. Both consist of a series of elements which are aligned parallel to the wave crests. In the case of the Salter Duck these are cam-shaped and floating on the surface, while the Bristol cylinder is fully submerged. Both have been shown to be able to absorb an incoming wave completely. The wave power is converted to electric power by means of a power take-off system that is hydraulic in both cases. As both devices move at approximately the wave induced water velocity, which is typically an order of magnitude smaller than the celerity, the devices need to feature a large surface area to convert appreciable amounts of power. This increases construction cost, reduces storm survival odds and has ultimately motivated the investigation of the cycloidal WEC described here. The fact that both devices require mooring to the ocean floor also hampers storm survival odds and precludes installation in very deep water.

Initial investigations of lift based wave energy conversion by means of a single hydrofoil were performed at TU Delft as early as the 1990s, both experimentally by Marburg [7] and numerically by van Sabben [8]. As noted by Hermans et al. [9], a major advantage of this approach over traditional wave energy converters is that the wave energy can be converted directly into rotational mechanical energy. This initial work demonstrated the feasibility of the approach, as well as the ability of a CycWEC to self-synchronize with the incoming wave in terms of rotational phase. However, the conversion efficiencies found both in the theoretical work and the wave tunnel experiments conducted at TU Delft were very small, in the order of few percent in experiments, with a theoretical maximum of 15%.

* Corresponding author. Tel.: +1 719 214 8815.
*E-mail address:* stefan@siegels.us (S.G. Siegel).

0141-1187/$ - see front matter © 2012 Elsevier Ltd. All rights reserved.
http://dx.doi.org/10.1016/j.apor.2012.07.003

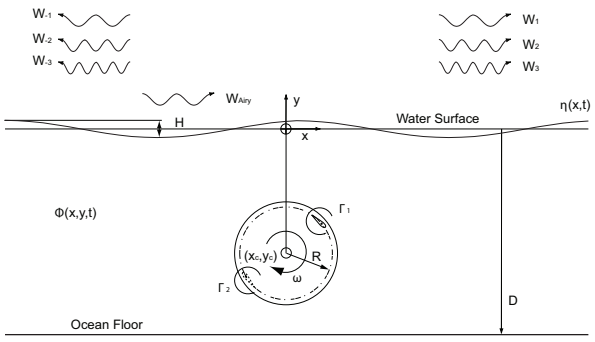


**Fig. 1.** Cycloidal wave energy converter geometry and generated waves.

Pinkster and Hermans [10] also demonstrated the use of a cycloidal turbine as a means of detecting wave direction and period with good accuracy.

A typical cycloidal WEC, as considered in this paper, is shown in Fig. 1. It features one or more hydrofoils attached parallel to a horizontally oriented main shaft at a radius $R$, rotating clockwise at angular speed $\omega$, and submerged a depth $y_c$, which is measured relative to a Cartesian coordinate system with $y = 0$ being the undisturbed free water surface. The hydrofoils are assumed to have a large span compared to their chord $c$, which is approximated by a large aspect ratio, which is the ratio between span and chord length. They are also assumed to be aligned parallel with the incident wave crests. The orientation (pitch) of each hydrofoil may be adjusted to produce the desired amount of wave height, which is proportional to the angle of attack as will be shown.

Based on the sketch in Fig. 1, a number of non-dimensional quantities emerge. The basic size of the wave energy converter is denoted by $2R/\lambda$, where the wave length $\lambda$ is the fundamental length scale. Consequently, the vertical position of the main shaft is denoted by $y_c$ and the wave height by $H$. It is also convenient for parameter studies to compare different size wave energy converters while keeping the distance between the water surface and the topmost point of the CycWEC foil path fixed, that is $|y_c + R| = const$. At any point on the free surface the vertical elevation is $\eta$ and peak-to-peak amplitude of the resulting wave field is denoted by $H$. The incoming wave $W_{Airy}$ is assumed to travel left to right, and waves generated by the cycloidal WEC traveling in the direction of the incoming wave receive a positive index (e.g., $W_1$) and are considered traveling down-wave; while waves traveling in the opposite direction are considered traveling up-wave and receive a negative index (e.g., $W_{-1}$).

The aim of the present work was to extend the experimental work presented at conferences in the recent past [11,12], as well as to compare the experimental results qualitatively and quantitatively to the results from numerical potential flow simulations as reported by Siegel et al. [13] and Jeans et al. [14]. This is done for operation of the CycWEC as both a wave generator as well as a wave energy converter following the rationale that efficient wave termination requires single sided wave generation. The results presented investigate the range of wave lengths for which a CycWEC of fixed size can efficiently generate and cancel incoming waves. This is of importance since in any real wave climate the wave height and frequency varies both from wave to wave, as well as from season to season. The impact of all design parameters, in particular submergence depth $y_c$, radius $R$, number of blades and pitch angle of the blades is investigated in detail and compared to simulation results. The parameter studies are conducted for rotation of the CycWEC with a fixed rotational period, or harmonic incoming waves of constant wave height, respectively. Thus, no feedback control is required and the CycWEC is operated with a fixed but adjustable phase shift relative to the incoming waves for wave cancellation. In further experiments, a feedback controller

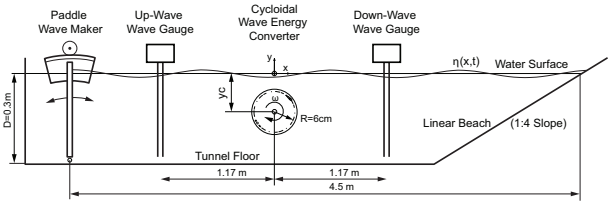


**Fig. 2.** Wave tunnel schematic – not to scale.

was employed to enable efficient interaction between the CycWEC and irregular waves. The feedback controller employed the signal of a single wave gauge located up-wave of the CycWEC in order to control rotation and pitch of the CycWEC blades based on this measurement in real time. Irregular waves were synthesized from simple harmonic waves with the wave power of each wave component determined from a Bretschneider distribution. The feedback controller employed the signal from a wave gauge positioned up-wave from the WEC, and controlled both rotation and blade pitch of the WEC. It is shown that efficient wave cancellation of irregular waves is possible with this setup.

## 2. Experimental setup

The tunnel used for testing the CycWEC was a 2D wave tunnel designed to provide a 1:300 scale model of a deep ocean wave. The full scale design deep ocean wave investigated numerically in [13] had a period of $T_{Airy} = 9$ s, a wave length of $\lambda_{Airy} = 126.5$ m, a wave height of $H = 3.5$ m, and power per meter of wave crest of $P = 105$ kW/m. It was represented in the present setup by a wave with a period of $T_{Airy} = 0.5$ s and wave length of $\lambda_{Airy} = 0.39$ m; at a typical wave height of $H = 20$ mm the scaled wave carried approximately $P = 192$ mW/m of wave power.

### 2.1. Wave tunnel

The wave tunnel is shown in a conceptual sketch in Fig. 2. The tunnel was designed for the generation and dissipation of waves with a period between $T = 0.2$ s and $T = 1.15$ s at wave heights up to $H = 5$ cm.

It had an overall length of 5 m, where 4.50 m were usable for wave experiments between the flap wave maker and the beach, a width of 0.55 m and a design water depth of 0.3 m. The width of the tunnel was increased by 50 mm on each side in the center test section, which allowed the drive system of the CycWEC to be placed outside of the wave testing area by means of false walls. At the right end of the tunnel, there was a linear beach with a 1:4 slope. For the design wave of $T = 0.5$ s and $H = 20$ mm, the reflection coefficient of the beach was measured by traversing two wave gauges using the approach described in [6] and found to be $C_r = 0.106$.

### 2.2. Irregular wave synthesis

The irregular incident wave field was created using a linear superposition of a finite number of linear Airy wave components using a flap type wave maker hinged at the bottom of the tunnel. The resulting surface elevation for a unidirectional deep ocean wave propagating in the $x$-direction and satisfying the linearized free surface boundary conditions was given in [15] to be

$$\eta_I(x,t) = \sum_{i=1}^{N_I} \frac{H_i}{2} \cos\left(k_i x - \omega_i t + \theta_i\right), \tag{1}$$

where $N_I$ was the number of regular wave components used to represent the irregular wave field, and $H_i$, $k_i$, $\omega_i$ and $\theta_i$ were the wave height, number, frequency and phase for component $i$, respectively.

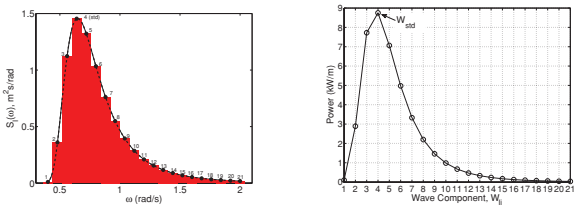


(a) Bretschneider energy spectrum for $H_s = 3.25$ m and $T_p = 9.7$ s (i.e. sea-state 5).

(b) Associated power of each of the 21 discrete wave components.

**Fig. 3.** Incident wave field modeled using the Bretschneider wave spectrum and 21 discrete wave components based on Airy wave theory.

The wave phase components $\theta_i$ were randomly generated from a uniform distribution between 0 and $2\pi$. The fidelity of the irregular wave field increased as the number of wave components was increased. According to [16], a minimum of 20 wave components were required for modelling a unidirectional irregular seaway.

The amplitude for component $i$ was based on a specified wave spectrum according to

$$a_i = \frac{H_i}{2} = \sqrt{2S_I(\omega_i)\Delta\omega_i}, \tag{2}$$

where $S_I$ was the spectral density and $\Delta\omega_i$ was the wave frequency interval for component $i$.

The 15th International Towing Tank Conference [17] defined the Bretschneider spectrum as

$$S_I(\omega) = \frac{486.0H_s^2}{T_p^4\omega^5}\ \exp\ \frac{-1948.2}{T_p^4\omega^4}, \tag{3}$$

where $H_s$ was the significant wave height and $T_p$ was the wave period associated with the peak energy. The Bretschneider wave spectrum for $H_s = 3.25$ m and $T_p = 9.7$ s (i.e. sea-state 5) is shown in Fig. 3(a). Also shown are the resulting wave components when the spectra was divided into 21 wave components with $\omega_{\min} = 0.4$ rad/s, $\omega_{\max} = 2.0$ rad/s, and $\Delta\omega_i = 0.08$ rad/s. Each wave component was identified numerically in Fig. 3(a) and is referred to as $W_{I1}$–$W_{I21}$ throughout the remainder of the paper. The amplitude of each wave was determined from Eq. (2). The wave power per unit length $P_i$ associated with each component was related to the wave height and period:

$$P_i = \frac{1}{32\pi}\rho g^2 H_i^2 T_i, \tag{4}$$

where $\rho$ was the density of water (assumed to be $\rho = 1000$ kg/m$^3$ for this study). Since the wave power scaled linearly with the wave period, higher harmonic waves of the same wave height contain less energy in proportion to their period. Also to be noted is the quadratic relationship between wave energy and wave height. For the full scale ocean wave, the power associated with each component wave in Fig. 3(a) is shown in Fig. 3(b). The total power of all 21 components was 41.79 kW/m and $W_{I4}$ had the peak power of all individual components with 8.75 kW/m.

The wave spectra with different numbers of component waves were scaled from full scale to tunnel scale using Froude scaling, where the wave period for the most dominant component $I_4$ was $T_4 = 0.5$ s. The corresponding significant wave height was $H_s = 15$ mm.

### 2.3. Cycloidal wave energy converter model

The CycWEC device is shown in Fig. 1. The only components interacting with the flow were the two hydrofoils spanning the tunnel. These hydrofoils were attached eccentrically at a radius $R = 60$ mm, and had a NACA 4 series hydrofoil of $c = 50$ mm chord length with a camber line curvature to match the radius of the circle on which they rotated. The hydrofoils had a resulting camber line displacement of 11%, and the maximum thickness of 15% was located at 50% chord.

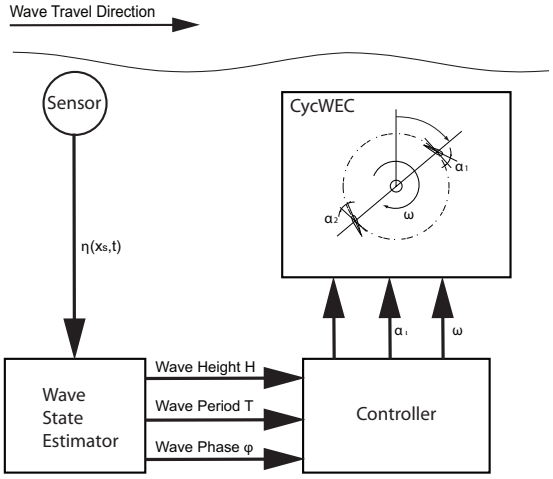


**Fig. 4.** Block diagram of sensing and feedback control approach.

This setup provided a zero-lift pitch angle of approximately 0° and was expected to behave like the familiar NACA 0015 in straight flow when rotating around a shaft.

The pitch angle of each blade was adjustable under computer control in real time. The blades could be adjusted over a range of approximately $\pm 20°$ with a positioning accuracy of $\pm 0.17°$. The sign convention for the pitch angle was chosen such that a rotation of the blade's leading edge toward the rotation center was negative, and a rotation outward, positive. For the present investigation, the blades were pitched in opposite direction at all times, which was found to provide the best performance in previous numerical studies.

The depth to which the rotational center of the CycWEC was submerged below the mean water surface, $y_c$, could be adjusted from the surface to $y_c = -0.1$ m, and was estimated to be accurate to $\pm 0.5$ mm. This allowed for investigation of the impact of changes in submergence depth on the performance.

Two wire type wave gauges for wave height measurements by electrical resistance were placed at a distance of 1.17 m up- and down-stream of the CycWEC main shaft. The overall accuracy and repeatability of the wave gauge measurements was estimated to be better than $\pm 0.1$ mm based on the repeat calibration results, or $\pm 0.5\%$ of the design wave height. The sample rate of the DAQ system was 100 Hz for both position control as well as data acquisition, where all measurements where synchronized. Typical measurement runs lasted 61 s, but only the final portion of the time signal after the flow had reached a steady state was used for data analysis by means of Fourier transform to determine wave heights.

### 2.4. Feedback control

A sketch of the overall control and estimation scheme is shown in Fig. 4. The signal from the up-wave wave gauge is used for feedback control, and processed first by the wave state estimator. The state estimation algorithm provides an approximation to the instantaneous wave height $H$, wave period $T$, and wave phase $\varphi$. These quantities are then used by the controller to prescribe the main shaft angle $\varphi$as well as the pitch of the blades. The following section describes the closed loop control approach further in detail.

Upon analysis of the up-wave wave gauge signal, the surface elevation measurement $\eta(t)$ displayed a periodic oscillation with unknown frequency and amplitude and was also corrupted by a small amount of high frequency noise as well as drift. Given a time history of the upstream measurement a relation was sought such that

$[\hat{\omega}(t)\hat{\phi}(t)\hat{H}(t)]^T = f([\eta(t), \eta(t-1), \ldots, \eta(t-n)]) + e(t)$ with minimal estimation error, $e(t)$. A typical Fourier analysis fell short because instantaneous phase information was lost in the decomposition. Other digital signal processing methods needed to be implemented. Because the upstream wave height measurement contained no negative frequency components, the signal could be expressed as an analytic signal:

$$\eta(t) = \frac{1}{2\pi}\int_0^\infty \eta(\omega) e^{j\omega t} \mathrm{d}\omega. \tag{5}$$

A complex representation of a periodic signal is $e^{j\omega t} = \eta(t) + i\hat{\eta}(t)$. The complex component of the analytic signal, which is unknown, is analogous to the Hilbert transformation, $\mathcal{H}[\bullet]$, of the real component; that is $\hat{\eta}(t) = \mathcal{H}[\eta(t)]$. The Hilbert transformation is a linear filter which produced a phase shift of $\pm(\pi/2)$ over all frequencies present in the signal, $\eta(t)$. In the time domain the transformation for this linear filter is identically the convolution with $1/\pi t$ which is shown as

$$\mathcal{H}[\eta(t)] = \frac{1}{\pi t} \times \eta(t) = \frac{1}{\pi}\int_{-\infty}^{\infty} \frac{\eta(t-\tau)}{\tau} \mathrm{d}\tau. \tag{6}$$

In the frequency domain the transform of the signal $f = 1/\pi t$ was

$$-j\,\mathrm{sgn}(f) = \begin{cases} -j & f > 0 \\ 0 & f = 0 \\ j & f < 0 \end{cases}. \tag{7}$$

The transfer function of this ideal filter does have a magnitude of one and a phase of $\pm(\pi/2)$ for $\pm\omega$, respectively. Because the Fourier transform is a non-causal transformation (dependent on previous, current and future measurements), an approximation to this transformation was necessary. Typical filters such as finite impulse response (FIR) and infinite impulse response (IIR) filters can be designed to simulate the response of $1/\pi t$. For the purposes of this paper, a three-stage cascading IIR filter was implemented to estimate the complex component of the Hilbert transformation with minimal (although non-linear) phase delays at the design frequency.

Now that the real and complex components of the analytic signal were known to within some degree of phase error, the instantaneous amplitude was estimated from the $L_2$ norm of the signals, i.e. $\hat{H}(t) = \| \eta(t) + i\hat{\eta}(t) \|_2$. The instantaneous phase was then computed as the angle between the real and complex estimate as, $\hat{\phi}(t) = \arctan(\hat{\eta}(t)/\eta(t))$, and the instantaneous frequency was calculated by the time derivative of the phase estimate. The state of the periodic signal measured at the up-wave location is now fully understood in terms of instantaneous phase, frequency and amplitude for single or multi-component wave trains.

The control scheme was very basic for the purposes of this paper. As the wave generation result showed, a very proportional relationship between angle of attack and generated wave height exists; thus, proportional control was used to prescribe the blade pitch $\alpha$, such that $\alpha_i(t) = P_g\hat{H}(t)$ with $P_g$ as the pitch gain. In order to implement rotary control for the wave energy converter the group velocity $C_g$ needed to be estimated and compensated for as a phase delay, i.e. the delay time necessary to propagate a wave from the up-wave measurement location to the CycWEC. The frequency of the passing wave obtained from the estimator and water properties made this a simple calculation. The time delays were then superimposed to control the rotational velocity of the main shaft in a stepwise fashion, such that $\phi(t) = \Phi(t) + (\eta_\lambda/C_g) + \theta_f$, where $C_g$ was the group velocity of the wave, and $\theta_f$ was the phase compensation of the cascading IIR filter.

## 3. Results

The experiments in this study were conducted in three stages. First, experimental runs were performed where the CycWEC was rotated in still water without any incoming waves. This setup allowed for evaluation of the wave generation capabilities of the CycWEC, which is important for incoming wave termination as discussed in Section 1. The results from these measurements are detailed in Section 3.1. Next, the CycWEC was exposed to a harmonic wave generated by the wave maker. The CycWEC was operated with a feedback controller that allowed for synchronization of the CycWEC with the incoming wave. In the final investigation, detailed in Section 3.3, the CycWEC was exposed to irregular waves following a Bretschneider distribution.

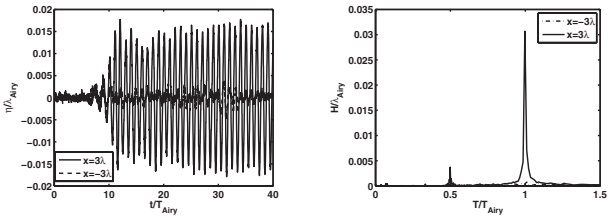


**Fig. 5.** Surface elevation (left) and power spectral density (right) for a CycWEC of size $2R/\lambda_{Airy} = 0.25$, submergence depth $|y_c + R|/\lambda_{Airy} = 0.016$, and blade circulation $T/\lambda^2_{Airy} = 0.025$. All waves are evaluated based on wave gauge measurements $x = \pm 2.5\lambda_{Airy}$ and time $t/T > 20$ after the start of the CycWEC.

### 3.1. Wave generation

The waves generated by a WEC operated without any incoming wave determine the overall ability of the WEC to efficiently cancel waves. An ideal outcome of a wave generation experiment would be a single sided wave of a single frequency, with no harmonic waves traveling in any other direction. If this is achieved in an incident wave field with a 180° phase shift to the incoming wave, wave termination with 100% efficiency can be accomplished. In the present experiment, the wave generation capabilities were evaluated by two wave gauges located up- and down-wave of the WEC, as shown in Fig. 2. A typical time signal from either of these wave gauges is shown in Fig. 5(left). The CycWEC was starting to rotate at a fixed frequency at time $t/T_{Airy} = 0$. It can be seen that the water surface up-wave is almost entirely still for all times. On the down-wave side, a mostly sinusoidal oscillation of the water surface can be observed, with approximately constant wave height after a few cycles. In order to quantitatively identify all present waves and their wave heights, a Fourier transform was employed, shown in Fig. 5(right). The first finding is that the frequency of the wave generated exactly matches the frequency of rotation of the WEC. The Fourier transform also reveals the presence of a first higher harmonic wave, which is attributed to the fact that at the wave height shown, a Stokes rather than an Airy wave would be expected. On the up-wave side, no distinct frequency was present in the wave gauge signal. The observed wave properties thus indicated that the CycWEC produced waves that were ideally suited for wave termination.

In the design of a CycWEC, three main geometric design parameters emerge. These are the diameter $2R$, the submergence depth of the unit below the water surface $y_c$, and the chord length of the hydrofoil, $c$. While the first two parameters are subject to Froude scaling, the chord length of the hydrofoil is linearly related to its ability to produce lift and thus circulation, $\Gamma$. To allow for comparison of all measured quantities with both experiments at different scales, as well as numerical simulations, the dimensions $2R$, $y_c$ and wave height $H$ were normalized by the wave length of an Airy wave, $\lambda_{Airy}$, while normalizing the circulation $\Gamma$ as $T/\lambda^2_{Airy}$. Since the interaction between the CycWEC and the free water surface was very sensitive to the distance between the hydrofoil and the surface at the top of the hydrofoil rotation, keeping this minimal submergence distance $|y_c + R|$ constant for investigations where the diameter of the CycWEC was varied relative to the wave length was advised. In this case, the non-dimensional

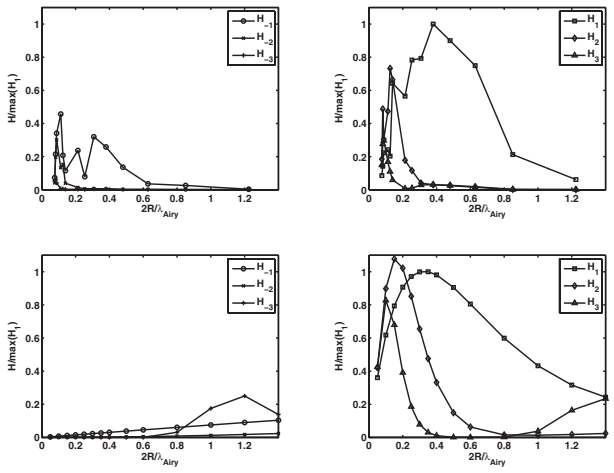


**Fig. 6.** Wave height experimental results (top) and simulation (bottom) as a function of device size for a minimum submergence $|y_c + R|/\lambda_{Airy} = 0.015$. All waves are evaluated at $x = \pm 3\lambda_{Airy}$ and $t/T = 30$ after the start of the cycloidal WEC.

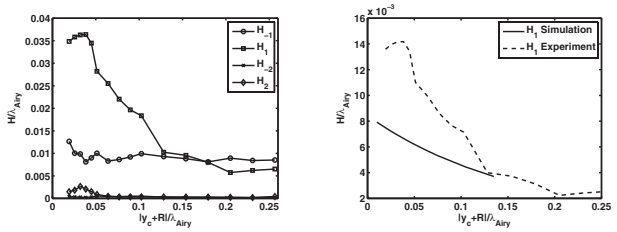


**Fig. 7.** Generated wave height in single blade experiment (left) and comparison of $H_1$ between single blade experiment and single vortex simulation (right) as a function of submergence depth $|y_c + R|/\lambda_{Airy}$ for a device size $2R/\lambda = 0.30$ and blade circulation of $T/\lambda^2_{Airy} = -0.05$ .

minimum submergence depth became $|y_c + R|/\lambda_{Airy}$.

The impact of relative size of the CycWEC on the heights of the generated waves is shown in the top portion of Fig. 6. The wave heights were determined based on Fourier analysis of the respective harmonic wave periods. For comparison, the results of the numerical simulations reported by Siegel et al. [13] are shown in the bottom portion of Fig. 6. For waves traveling in the down-wave direction with a positive index, both simulation and experiment showed significant wave heights mainly for the fundamental wave, $H_1$. The size at which this fundamental wave reached its maximum wave height was about $2R/\lambda_{Airy} = 0.3$ in both experiment and simulation. The harmonic waves $H_2$ and $H_3$ reached their respective maxima at smaller relative sizes, $2R/\lambda_{Airy} = 0.15$ and $2R/\lambda_{Airy} = 0.1$, respectively. The reason for this was that maximum wave generation occurred when a match between the velocity of the hydrofoil travel, and the celerity of the waves generated was achieved (i.e., $\omega R = C$ assuming Airy wave theory). For the fundamental wave this corresponded with $2R/\lambda_{Airy} = 1/\pi$ , which was the optimal device size for wave generation. Since the harmonic waves had a celerity of one half and one third of the celerity of the fundamental wave, the match occurred at respectively smaller size ratios. While there was good agreement between experiment and simulation as far as the size ratio of the maxima was concerned, the relative height of these peaks was different. In particular, the experiment showed smaller wave heights for the harmonic waves $H_2$ and $H_3$. This was most likely due to the fact that these higher frequency waves were approaching the limit for gravity waves and were transitioning to waves with surface tension as the main restoring force, and were thus subject to higher dissipation. This effect was not present in the simulations, where surface tension was neglected. For the same reason, the harmonic wave $H_{-3}$ was all but absent in the experimental results, while being the most dominant up-wave traveling wave in the numerical data. The experimental data instead showed relatively large fundamental wave heights $H_{-1}$ traveling up-wave, which were most likely due to reflections from the beach. It should be noted that in the experimental investigations shown in Fig. 6 the pitch angle of the WEC blades along with the WEC geometry was kept constant, while the rotational rate was changed to achieve the different size ratios $2R/\lambda_{Airy}$. This caused the circulation to change in proportion to the hydrofoil velocity. In the simulations, the radius was varied while keeping the circulation constant. To make both data sets comparable, the experimental data were scaled linearly to adjust for the changes in circulation. As will be shown later, both experimental and simulation results justify linear scaling of wave height with circulation.

A second parameter study was performed to determine the impact of submergence depth on wave heights generated. Fig. 7 shows the wave heights as a function of non-dimensional minimum submergence depth $|y_c + R|/\lambda_{Airy}$ on the left, and a comparison of the fundamental wave height to the numerical simulations on the right. The experimental data showed fundamental wave $H_1$ to be strongly increasing in wave height for decreasing submergence depths up to $|y_c + R|/\lambda_{Airy} = 0.04$, beyond which the wave height was slightly reduced. The up-wave traveling fundamental wave was almost constant for the entire submergence depth range investigated. The comparison to the numerical single-point vortex simulations showed a much larger increase in the experiment than in the simulations for submergence depths less than $|y_c + R|/\lambda_{Airy} = 0.13$. This effect was most likely due the fact that the hydrofoil in the experiment had a significant chord length which was not captured in the single point vortex simulations. Limited data presented in Fig. 14 of Siegel et al. [13] that showed the impact of finite chord length indicated an increase in wave height with chord length to almost double for the present chord length to wave length ratio of $c/\lambda_{Airy} = 0.12$. Thus, the larger increase in wave height compared to the single point vortex simulation for submergence depths of $0.04 < |y_c + R|/\lambda_{Airy} < 0.13$ appeared to be mostly caused by the finite length of the hydrofoil chord. However, the simulation data with a linear boundary condition did not predict the reduction in wave height beyond $|y_c + R|/\lambda_{Airy} = 0.04$. At this very close distance between hydrofoil and water surface, most likely non-linear surface interaction effects dominated the flow behavior.

The third portion of wave generation investigations concerned the impact of hydrofoil pitch angle on generated wave height. Fig. 8(left) shows the wave heights generated as a function of blade pitch angle $\alpha$. For all investigated size ratios, a minimum wave height was seen to occur at zero pitch. In this situation, the remaining wave generation was thus entirely caused by the hydrofoil thickness displacing the water surface, since no lift and thus circulation was generated. For negative pitch angles, the hydrofoil lift increased almost linearly up to stall, which occurred at the Reynolds numbers investigated here at about $\alpha = 7.5^\circ$. However, the increase in wave height followed a different slope for the different size ratios. This change was due to the fact that the circulation for each size ratio was different for a fixed pitch angle, as the rotational velocity varied. Fig. 8 right shows that all data for the different size ratios collapsed onto a single line, when the wave height was plotted as a function of non-dimensional circulation instead; at least up to hydrofoil stall. This finding was in good agreement with the simulation data, which showed that the generated wave height was a linear function of hydrofoil circulation (see Fig. 7 in Siegel et al. [13]). It is worth noting that as opposed to a symmetric hydrofoil in a uniform stream, where stall occurs at same pitch angles for both negative and positive pitch directions, the stall in the positive pitch direction for the rotating hydrofoil appeared delayed or eliminated. Since the entire setup in the present investigation was asymmetric due to the presence of the free water surface, asymmetric stall can be expected. On the other hand, the slope of the wave

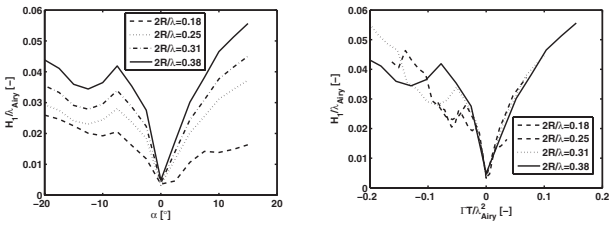


**Fig. 8.** Generated fundamental wave height $H_1$ as a function of blade pitch angle (left), and blade circulation $\Gamma$ (right). Submergence depth $|y_c + R|/\lambda_{Airy} = 0.015$.

**Fig. 9.** Picture of wave cancellation from side. Incoming wave period $T = 0.5$ s, wave height $H_{-1}/\lambda_{Airy} = 0.056$, traveling left to right. The CycWEC has two blades, feedback phase $\theta = 197^\circ$, blade pitch gain $G_p = 400^\circ/\text{m}$, submergence $|y_c + R|/\lambda_{Airy} = 0.038$.

height curve remains symmetric for pitch angles below stall, again in agreement with simulation data.

In summary the results obtained from the harmonic wave generation experiments are in good agreement with those from the numerical simulations, and indicate that wave cancellation is achievable if the CycWEC can be successfully synchronized to the incoming wave. The next section details the experimental results from wave cancellation.

### 3.2. Harmonic wave cancellation

In order to achieve wave cancellation, the CycWEC needs to rotate in sync with the incoming wave, with a phase shift such that the wave generated by the CycWEC is exactly out of phase with the incoming wave (phase shift of $\varphi = 180^\circ$). To synchronize the CycWEC with the incoming wave, the signal from the up-wave gauge was used to estimate the wave period, amplitude and phase of the incoming wave. A phase estimator as described in the feedback control section was used to accomplish this. A linear feedback law then adjusted the rotation of the main shaft and pitch angle of the blades for optimal wave cancellation. Figs. 9 and 10 show a side view and view in the up-wave direction of the wave flume during the stabilized portion of a feedback controlled wave cancellation experiment. The CycWEC was installed in the center of the portion of the image that was blocked from view by the CycWEC support system in Fig. 9. While the incoming waves can be seen up-wave of the CycWEC in the left portion of the image, there are only small amplitude waves of short wave length visible on the right, down-wave side of the CycWEC indicating successful wave cancellation.

Quantitative measurements of the feedback controlled wave cancellation are shown in Fig. 11. The wave gauge signals confirm the reduction in wave height achieved by the CycWEC, which is in the order of about 80% of the incoming wave height. Any harmonic waves present carry negligible amounts of energy, and with the wave energy being proportional to the square of the wave height, about 95% of the incoming wave energy is terminated at the CycWEC. A corresponding Fourier transform is shown in Fig. 12, and was used to determine the exact wave heights.

It is of interest to investigate the sensitivity of the wave cancellation to errors in phase. The results from a study varying the feedback phase are shown in Fig. 13. While the incoming wave height $H_{-1}$ remains approximately constant independent of feedback phase, the height of the remaining wave $H_1$ down-wave of the CycWEC depends

**Fig. 10.** Picture of wave cancellation from downwave above. For experimental parameters see caption of Fig. 9.

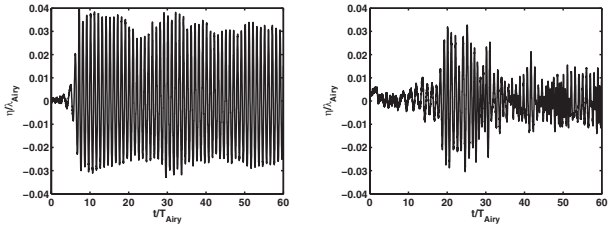


**Fig. 11.** Up-wave (left) and down-wave (right) water surface elevation during feedback controlled wave cancellation. For experimental parameters see caption of Fig. 9.

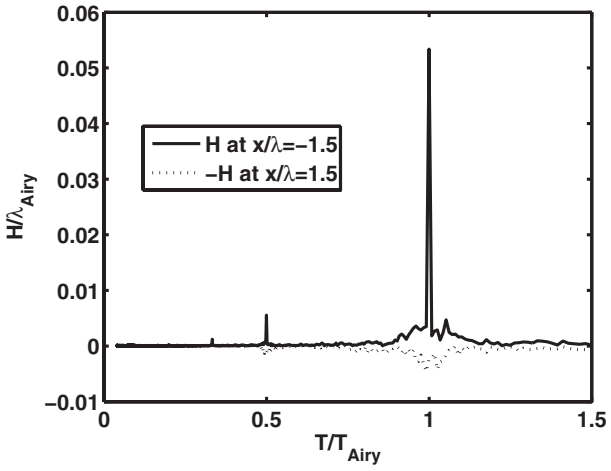


**Fig. 12.** Power spectral density of the surface elevation at the up-wave and down-wave wave gauge. For experimental parameters see caption of Fig. 9.

strongly on the feedback phase, showing a minimum remaining wave height at a phase shift of about $\varphi = 198^\circ$.

While successful termination of a harmonic wave is an encouraging result, the ultimate goal of wave energy conversion is to extract energy from irregular ocean waves, where both wave height and period vary from one wave to the next. The following section presents initial results for cancellation of waves following a Bretschneider distribution of wave power for the individual component waves.

### 3.3. Irregular wave cancellation

For the first experiments targeting cancellation of irregular waves, a wave signal was synthesized from 7 components of a Bretschneider distribution. These components were added to each other with a random phase shift, resulting in a time signal as shown in Fig. 14(left). The CycWEC was operated with the same controller used for the harmonic

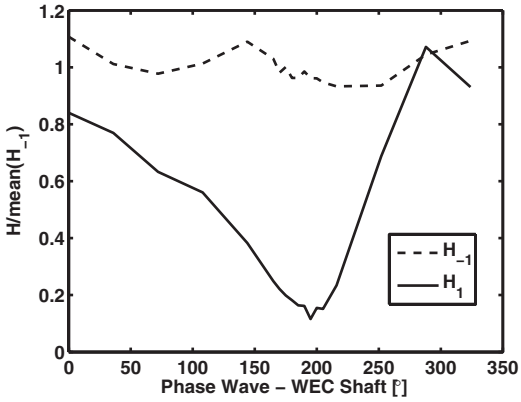


**Fig. 13.** Fundamental wave heights as a function of feedback phase $\theta$. Incoming wave period $T = 0.5$ s, WEC has two blades, blade pitch gain $G_p = 400^\circ/\text{m}$, submergence $|y_c + R|/\lambda_{Airy} = 0.026$ mm.

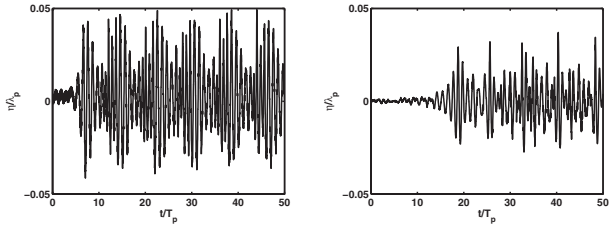


**Fig. 14.** Up-wave (left) and down-wave (right) water surface elevation during feedback controlled cancellation of a irregular Bretschneider wave with 7 components, $T_p = 0.5$ s, $H_s/\lambda = 0.038$.

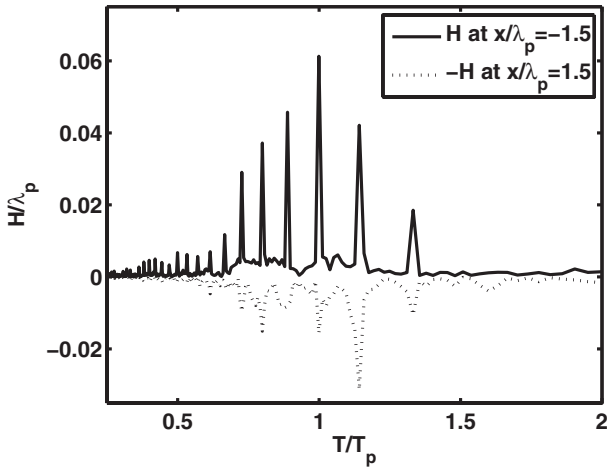


**Fig. 15.** Power spectral density of the surface elevation at the up-wave and down-wave wave gauge during cancellation of a 7 component Bretschneider spectrum irregular wave. Note that the spectrum of the down-wave wave gauge is plotted negative.

wave cancellation experiments described in the previous section. The right portion of Fig. 14 shows that down-wave of the CycWEC the wave heights are greatly reduced in amplitude beyond $t/T_p = 30$. Using the spectral analysis data shown in Fig. 15, the overall efficiency for this particular wave cancellation effort was determined to be 77%. Also notable is that every individual component wave is reduced in wave height, and no additional harmonic waves can be observed.

Wave cancellation experiments were conducted with different numbers of component waves and have been published in Siegel et al. [18]. The corresponding simulations can be found in Jeans et al. [14]. Both simulations and experiments yielded similar overall efficiencies ranging from about 60% to 80%. This posed the question why the irregular cancellation data showed less overall performance than the harmonic cancellation. An investigation into this found feedback control issues hampering performance, which, once improved, yielded irregular efficiencies on par with harmonic cancellation performance. Initial results from simulations with the improved controller are reported in Fagley et al. [19]. It is planned to reproduce these numerical results in experimental work in the near future.

## 4. Conclusion

A cycloidal wave energy converter (CycWEC) can be used both as an efficient wave maker, as well as a wave termination device when synchronized to an incoming wave by means of feedback control. Results from two-dimensional wave flume experiments at a scale of 1:300 with CycWECs featuring both a single hydrofoil as well as two hydrofoils spaced 180° apart are presented. The CycWEC was operated under feedback control with a resistive wave gauge located upwave of the CycWEC as the sole input to the estimator and controller. The experimental results presented here are in good agreement with numerical simulations published earlier by Siegel et al. [13], with any discrepancies between experiment and simulation related to inherent limitations of either approach.

### 4.1. Wave generation

For wave generation, it was possible to create a single Airy type wave that only traveled in one direction, with no waves generated in the other direction. The direction of travel was controlled by the rotation direction, while the wave height varied linearly with hydrofoil circulation up to hydrofoil stall. For a single blade WEC the resulting wave field was decomposed into the fundamental wave traveling upwave and two higher harmonics of much smaller amplitude traveling both up- and down-wave. The optimal device size was determined to be $2R/\lambda_{Airy} = 1/\pi$, corresponding to an exact match between the hydrofoil rotational velocity and the wave speed of the generated wave. A significant improvement in the wave field was achieved using a WEC with two hydrofoils spaced 180° apart with equal but opposite circulation. For this configuration, the harmonic wave of twice the fundamental frequency was reduced to negligible amplitudes, resulting in a significantly improved wave field for wave termination applications.

### 4.2. Wave cancellation

The single sided wave generated by the CycWEC was perfectly suited to extract energy from an incoming plain Airy wave. In order to achieve this, the motion of the CycWEC needed to be synchronized in frequency and phase locked to the incoming wave, and the circulation of the converter's hydrofoils needed to be adjusted to produce a wave of matching amplitude by means of feedback flow control. If this was accomplished, more than 95% of the incoming wave energy could be extracted from the wave achieving wave termination of harmonic waves. When the CycWEC was exposed to irregular waves consisting of a larger number of Airy waves following a Bretschneider distribution in wave power, between 60% and 80% of the wave energy could be extracted.

Based on the data presented in the preceding section, it was concluded that the CycWEC under feedback control was able to efficiently cancel both harmonic and irregular waves.

### 4.3. Comparison to numerical results

The overall agreement between the numerical potential flow simulations presented by Siegel et al. [13] and the data presented here were very good, and demonstrated the capability of the CycWEC to efficiently extract energy from irregular deep ocean waves in both experiment and simulation. Both experiment and simulation indicate

the same optimal size of an efficient CycWEC of $2R/\lambda = 1/\pi$. However, due to inherent limitations of the experiment as well as the simulation, differences in the data can be found close to the surface, where non-linear effects cause different wave heights to be found in experiment and simulation. While the simulation shows a continuous increase in wave height as the WEC is moved closer to the surface, the experiment finds a reduction for very small submergence depths. This is most likely due to the non-linear interaction between surface and hydrofoil. Another difference was about the distinctly smaller amplitudes for higher harmonic waves found in the experimental data. As the frequencies of these harmonic waves exceed the frequency range for which gravity waves can be expected, this difference is most likely a limitation of the relatively small scale of the experiment.

## Acknowledgments

The authors would like to acknowledge the fruitful discussions with their colleagues at the Air Force Academy, most importantly Dr. Seidel for his help in proofreading the manuscript. This material is based upon activities supported by the National Science Foundation under Agreement No. ECCS-0801614, monitored by Dr. George Maracas. Any opinions, findings, and conclusions or recommendations expressed are those of the authors and do not necessarily reflect the views of the National Science Foundation.

## References

[1] Boyle G. Renewable energy - power for a sustainable future. Oxford University Press; 2004.
[2] McCormick M. Ocean wave energy conversion. John Wiley & Sons; 1981.
[3] Mei CC. The applied dynamics of ocean surface waves. John Wiley & Sons; 1983.
[4] Cruz J. Ocean wave energy: current status and future prepectives. Springer-Verlag; 2008.
[5] Salter SH. World progress in wave energy-1988. International Journal of Ambient Energy. 1989;10(1):3–24.
[6] Evans DV, Jeffrey DC, Salter SH, Taylor JRM. Submerged cylinder wave energy device: theory and experiment. Applied Ocean Research. 1979;1(1):3–12.
[7] Marburg C. Investigation on a rotating foil for wave energy conversion. Master's thesis. TU Delft; 1994.
[8] van Sabben E. De in het snelheidsveld van lopende golven ronddraaiende plaat; invloed op het vrije vloeistofoppervlak. Master's thesis. TU Delft; 1987.
[9] Hermans AJ, van Sabben E, Pinkster J. A device to extract energy from water waves. Applied Ocean Research Computational Mechanics Publications. 1990;12(4):5.
[10] Pinkster J, Hermans AJ. A rotating wing for the generation of energy from waves. In: 22nd IWWWFB Conference. 2007.
[11] Siegel SG, Fagley C, Roemer M, McLaughlin T. Experimental wave cancellation using a cycloidal wave energy converter. In: 9th European Wave and Tidal Energy Conference (EWTEC). 2011.
[12] Siegel S., Roemer M., Imamura J., Fagley C., Mclaughlin T. Experimental wave generation and cancellation with a cycloidal wave energy converter. In: 30th international conference on ocean, offshore and arctic engineering (OMAE). OMAE2011-49212. 2011.
[13] Siegel SG, Jeans T, McLaughlin T. Deep ocean wave energy conversion using a cycloidal turbine. Applied Ocean Research. 2011;33(April (2)):110–119.
[14] Jeans T, Siegel SG, Fagley C, Seidel J. Irregular deep ocean wave energy conversion using a cycloidal wave energy converter. In: 9th European wave and tidal energy conference (EWTEC). 2011.
[15] Newman JN. Marine hydrodynamics. MIT Press; 1977.
[16] McTaggart K. Modelling and simulation of seaways in deep water for simulation of ship motions. Tech. Rep. Tech. Rep. DRDC Atlantic TM 2003-190. Defence R&D Canada - Atlantic; September 2003.
[17] ITTC Seakeeping Committee Report. In: 15th international towing tank conference; 1978.
[18] Siegel S, Fagley C, Roemer M, Mclaughlin T. Experimental investigation of irregular wave cancellation using a cycloidal wave energy converter. In: 31st international conference on ocean, offshore and arctic engineering (OMAE). OMAE2012-83388. 2012.
[19] Fagley C, Siedel J, Siegel S. Computational investigation of irregular wave cancellation using a cycloidal wave energy converter. In: 31st international conference on ocean, offshore and arctic engineering (OMAE). OMAE2012-83434. 2012.